RSC Advances

This article can be cited before page numbers have been issued, to do this please use: W. Song, S. Tao, Y. Yu, X. Du and S. Wang, *RSC Adv.*, 2016, DOI: 10.1039/C6RA12088A.

ROYAL SOCIETY OF CHEMISTRY

www.rsc.org/advances

View Article Online
DOI: 10.1039/C6RA12088A

Journal Name

ARTICLE

Preparing Magnetic Multicomponent Catalysts via the Bio-inspired Assembly For Heterogeneous Reactions

Received 00th January 20xx,
Accepted 00th January 20xx

DOI: 10.1039/x0xx00000x

www.rsc.org/

Wentong Song, Shengyang Tao*, Yongxian Yu, Xuanlu Du and Shuo Wang

This article reports a facile synthetic approach for preparing magnetic porous catalysts, on which various inorganic compounds are alternately loaded using a pyrogallic acid (PG)-assisted layer-by-layer (LbL) coating. The PG forms an adhesion and reductive layer on the surface of hierarchically porous silica, and Pd, Al_2O_3, ZrO_2, or FeOx can then be introduced on the surface of the material. Compared with the conventional impregnation method, the PG layer obviously improves the dispersion of catalysts and greatly reduces the blocking of the pores, which is caused by the formation of metal oxide catalysts. At the same time, the reduction properties of the layer help to reduce the diameter of the Pd nanoparticles to 5 ± 1.3 nm. The Fe^{3+} ions are partially reduced into Fe^{2+} by the PG layer to form Fe_3O_4, which endows the porous catalysts with a magnetic separation property. The synthesized multicomponent catalysts show excellent catalytic activity for various reactions, including Suzuki Miyaura coupling, reduction, Knoevenagel condensation and Friedel–Crafts alkylation reactions. The TOF values show an improvement of 2 to 4 times over those of the catalysts prepared by the traditional impregnation method. The multicomponent magnetic catalysts also exhibit superior catalytic performance for many one-pot multistep cascade reactions.

Introduction

Uniformly dispersing nano-sized inorganic catalysts on the surface of porous carriers is important for improving the efficiency of the catalyst in heterogeneous catalysis,[1] yet still represents a significant challenge.[2, 3] Reducing the size of catalytic particles increases the utilization rate of the atoms, which reduces the amount of expensive catalysts required, including Au, Pt and Pd.[4-8] In recent years, researchers have found that the activity of catalysts can be controlled by varying the surface properties of the support materials.[9-11] Porous silica is one of the most commonly used catalyst support materials due to its large surface area, tunable pore structure and chemical stability.[12, 13] Immobilization of the inorganic catalysts on the surface of the porous silica support is usually achieved using the impregnation method with calcination treatment. However, this normal impregnation method makes it difficult to control the formation process of the inorganics in the pores. Large particles are easily generated due to interface migration and aggregation, but this lowers the dispersibility of the catalysts and can even block the inner pores. Obviously, the catalysts' active sites cannot then be used effectively.[14] Therefore, the particle size and distribution of the active catalytic compounds on the surface of porous silica become the key factors in determining the reactivity and selectivity of catalysts. Furthermore, many multistep cascade reactions need different catalysts. The integration of various inorganics on one porous support with high dispersion is therefore meaningful work, but difficult to achieve.[15, 16]

In nature, biological systems often exhibit complicated compositions and multiple functions.[17, 18] In these systems, it is common for inorganics to self-assemble with the assistance of organic molecules. For example, shells, which have high hardness and ideal stability, are formed merely by the LbL assembly of $CaCO_3$ nanoparticles and proteins.[19, 20] Mimicking this biomineralization process can help researchers to develop excellent organic-inorganic hybrid materials.[21-26] Further, incorporation of a magnetic component (e.g. Fe_3O_4) to provide an additional function to the original material has been widely used and there were many reports on the applications of magnetite nanocomposite material for catalysts.[27-31] Lately, Messersmith et al. successfully introduced inexpensive plant polyphenols onto solid surfaces, and the polyphenol film showed adsorption and reduction properties with metal ions.[32] Therefore, inspired by the unique adhesion and reduction properties of plant polyphenols in nature, we developed a general, green chemistry approach for the immobilization of inorganic catalysts. Therefore, in our work, catalytic metal oxides are loaded on HPS by polyphenols. This approach is more facile, low-cost and environmental friendly. In addition, it can be extended to the immobilization of more catalysts on various materials for various reactions. We used PG as an

Department of Chemistry, Dalian University of Technology, Dalian 116024, Liaoning, P.R. China.
E-mail: taosy@dlut.edu.cn; Fax: +86-411-84986035; Tel: +86-411-84986035
Electronic Supplementary Information (ESI) available: [details of any supplementary information available should be included here]. See DOI: 10.1039/x0xx00000x

View Article Online
DOI: 10.1039/C6RA12088A

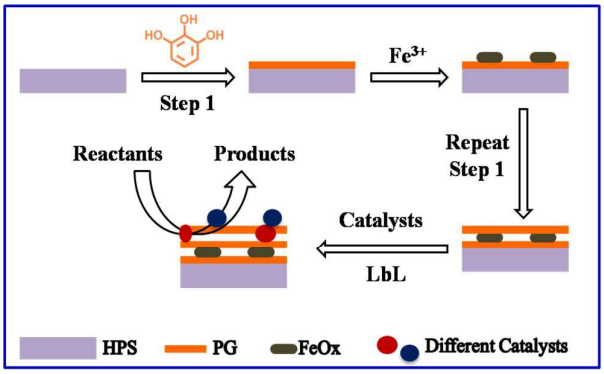

Scheme 1. Pyrogallic acid (PG) as an adhesion layer to combine the LbL coating and impregnation method. Then, magnetic component and many other inorganic compounds were successfully intergraded in hierarchically porous silica (HPS).

adhesion layer to combine the LbL coating and impregnation methods in this study. Then, a magnetic component and many other inorganic compounds were successfully intergraded in the hierarchically porous silica (HPS) (Scheme 1). HPS, which has both macro and meso pores, has the advantages of a large surface area and high molecular diffusion, which are beneficial for the loading of catalysts and transfer of reactants. The PG layer could strongly adhere to almost all types of surfaces. Although one side of the PG layer bound to the silica surfaces through covalent and noncovalent interactions, it further immobilized various kinds of metal ions through coordination or reduction. The selective chemical adsorption led to uniform inorganic compounds. After the calcination, the dispersion of catalytic materials was considerably improved. Surprisingly, through the reducibility of PG, the magnetic element (FeOx) was also fabricated in the porous silica using the LbL coating. The multicomponent catalysts showed excellent catalytic activity for several reactions, even including cascade reactions. High conversion ratios, selectivity and TOF values were achieved, indicating that they are highly efficient catalysts.

Experimental Section

Reagents and materials. Tetramethoxysilane (TMOS) was bought from the Chemical Factory of Wuhan University (Wuhan, China). PEG (polyethylene glycol, Mw=10,000), NaOH, Na_2SO_4 were bought from the Sinopharm Chemical Reagent Co., Ltd. N, N-Bis (2-hydroxyethyl) glycine, pyrogallic acid, aluminium isopropoxide, zirconium n-propoxide, iodobenzene, phenylboronic acid, indoles, chalcones, benzaldehyde dimethylacetal, 4-nitrophenol (4-NPh), 4-aminophenol (4-APh) and sodium borohydride were bought from Aladdin Chemical Co., Ltd. Acetic acid, nitric acid, anhydrous ethanol, hydrochloric acid were purchased from Fuyu Fine Chemical of Tianjin Co., Ltd. Malononitrile was purchased from Shanghai Kefeng Chemical Reagents Co., Ltd. Benzaldehyde, n-propyl alcohol, n-butyl alcohol, methylbenzene and diethyl ether were purchased from Tianjin Kemiou Chemical Reagent Co., Ltd. Ethyl cyanoacetate was purchased from J & K Scientific Ltd. All the reagents mentioned above were used without further purification.

Synthesis of HPS support. The HPS was prepared and modified by previously reported method.[33] The experimental details are shown below: Firstly, PEG (8.85 g) and acetic acid (10 mM, 75 mL) were mixed together and stirred to get a homogeneous solution. Subsequently, TMOS (30 mL) was added and stirred for about 10 min for hydrolysis at 0 ℃. Then the semitransparent sol was transferred into polythene (PE) tubes sealed for gelation and aged (36 h) at 40 ℃ after which the resultant gels were treated by 1 M ammonium hydroxide solution at 110℃ for 9 h. Thirdly, the porous monolithic materials was cooled down to room temperature and impregnated into aqueous solution of nitric acid (0.1 M) to pH = 7.0 and then evaporation-dried at 60 ℃ after washing by deionized water. The required HPS support was obtained by calcination at 650 ℃ for 5 h in air.

Preparation of PG modified silica (HPS-PG). The as-made HPS (1.0 g) were crushed and sieved to collect 600–850 μm particles and then immersed into bicine buffer solution (pH = 7.8, 0.1 M, 10 mL) containing PG (0.1 mg mL^{-1}) at room temperature for 24 h, the obtained solid particles (named as HPS-PG) were washed by water and dried over night.

In-situ generation of Pd nanoparticles modified silica support. HPS-PG (1.0 g) particles was added into aqueous solutions of $PdCl_2$ (15 mM, 10 mL) at room temperature for 6 h, the solid was washed with water, and dried in vacuum then the HPS-PG-Pd sample was obtained and after calculation we name it as HPS-C-Pd. Similarly uncoated silica-supported Pd nanoparticles were fabricated using the same procedures and after calcination we name it as HPS-Pd.

In-situ generation of metal oxides modified silica support. HPS-PG (1.0 g) immersed into aqueous solutions of $Fe(NO_3)_3$ $9H_2O$ (0.2 M, 10 mL) , iso-Propyl alcohol solution of aluminium isopropoxide (10 mM, 10 mL) and n-propanol solution of zirconium n-propoxide (20 mM, 10 mL), respectively at room temperature for 24 h, the solid was washed with ethanol, and dried in vacuum at 40 ℃. The resultant modified silica supports were named as HPS-PG-Fe, HPS-PG-Al and HPS-PG-Zr. The calcining process was carried out to obtain the HPS-C-FeOx, HPS-C-Al_2O_3 and HPS-C-ZrO_2. Similarly, uncoated silica-supported metal oxides were fabricated using the same procedures and after calcination we name them as HPS-FeOx, HPS-Al_2O_3 and HPS-ZrO_2, respectively.

Preparation of bi-functional materials by LbL coating. The preparation of HPS-C-FeOx-C-Pd, HPS-C-FeOx-C-Al_2O_3 and HPS-C-FeOx-C-ZrO_2 were the same as HPS-C-Pd, HPS-C-Al_2O_3 and HPS-C-ZrO_2, respectively except the HPS-PG-FeOx was used as support. The uncoated HPS-C-FeOx was also used to support Pd, Al_2O_3 and ZrO_2 with the same procedure and we called them HPS-C-FeOx-Pd, HPS-C-FeOx-Al_2O_3 and HPS-C-FeOx-ZrO_2.

Preparation of multi-functionally and magnetically recoverable catalysts by LbL coating. HPS-C-FeOx-C-Al_2O_3 was used as support, coated with PG, followed by immersed into n-propanol solution of zirconium n-propoxide (20 mM, 10 mL) and aqueous solutions of $PdCl_2$ (15 mM, 10 mL), respectively. With the procedure mentioned above and named them as

View Article Online
DOI: 10.1039/C6RA12088A

HPS-C-FeOx-C-Al_2O_3-C-ZrO_2 and HPS-C-FeOx-C-Al_2O_3-C-Pd. All the above mentioned calcinations were carried out in a tubular furnace under nitrogen condition. The temperature program was from room temperature to 550 ℃ with a ramp of 3 ℃ min^{-1} and maintenance for 6 h.

Characterization. The microscopic features of the samples were taken with a QUANTA 450 scanning electron microscope (SEM) at 30 kV. Transmission electron microscope (TEM) images were obtained with a Tecnai F30 electron microscope equipped operates at 300 kV accelerating voltage and equipped with Schottky Field emission gun (FEG). X-Ray diffraction (XRD) patterns were obtained on a Rigaku D/MAX-2400 X-ray powder diffraction (Japan) using Cu Kα radiation, operating at 40 kV and 10 mA. The surface elements were analyzed by X-ray photoelectron spectroscopy (XPS, Shimadzu KROTAS AMICUS spectrometer).The nitrogen adsorption and desorption isotherms were measured at 77 K using an ASAP 2010 analysis instrument. The specific surface areas were calculated by the Brunauer-Emmett-Teller (BET) method and the pore size were calculated using the Barrett-Joyner-Halenda (BJH) model. FT-IR spectra (4000-400 cm^{-1}) were collected on a Nicolet Avatar 360 FT-IR spectrometer. Thermal gravimetric analysis (TGA) was carried out using TGAQ600 ramp 10 ℃ min^{-1} to 500 ℃. We used UV1000 spectrophotometer to measure the conversion of p-Nitrophenol in the solutions. Gas chromatography (GC-7900) equipped with a capillary column (PEG-20M, 30.0 m×320 mm×0.25 mm) and an FID detector was used to measure the conversion of the Reactant. The magnetic measurements were performed on a super conducting quantum interference device vibrating sample magnetometer (Quantum Design SQUID) at 300 K. ^{1}H-NMR spectra were measured on a Varian INOVA 400M spectrometer with chemical shifts reported in ppm.

Catalytic Suzuki-Miyaura cross-coupling reactions. In a typical run, iodobenzene (2.0 mmol), phenylboronic acid (2.4 mmol) were added to 40 mL of deionized water, then NaOH (8.0 mmol) was added and stirred at 80 ℃ until the chemicals are completely dissolved. Then catalyst (0.2 g) was added to the stirred solution in one portion, and the reaction mixture was stirred for another 3 h. After the mixture had cooled to room temperature, the reaction mixture was diluted with diethyl ether (2 × 20 mL), dried with excessive Na_2SO_4, and concentrated under reduced pressure to yield the final product.

Catalytic activities for nitro reduction reactions. In a typical reduction protocol, 50 mg of catalyst was added to 10 mL water containing 0.1 mmol of nitro-compound and 1.3 mmol of $NaBH_4$. The mixture was vigorously stirred at room temperature for 10 min. The reaction was monitored by UV-vis spectroscopy. The bright yellow solution gradually faded as the reaction proceeded.

Catalytic activities for Knoevenagel condensations. Reactions were performed with benzaldehyde and ethyl cyanoacetate at 80 ℃ or malonitrile at 25 ℃ in DMF. In a typical run, the catalyst (0.2 g), benzaldehyde (0.1 mol), ethyl cyanoacetate or malonitrile (0.11 mol), and DMF (15 mL) were mixed in a flask connected to a cooling condenser. Then the flask was immersed into an oil bath equipped with a magnetic stirrer under N_2.

Catalytic for Friedel–Crafts reactions. Friedel-Crafts alkylation of indoles with chalcones was carried out. In a typical synthesis, indole (2 mmol), chalcone (3 mmol), catalyst (0.1 g), and methylbenzene as solvent (20 mL) were mixed in a flask connected to a cooling condenser. Then the flask was immersed into an oil bath equipped with a magnetic stirrer at 110 ℃ for 6 h.

Catalytic the cascade reactions of Knoevenagel condensation coupled with subsequent hydrogenation process. In a typical procedure, the catalysts（0.1 g） were dispersed into 15 mL DMF, followed by adding 4-nitrobenzaldehyde (0.2 mmol) and malononitrile (0.21 mmol). Next, the obtained solution was stirred in a stainless-steel autoclave at 80 ℃ for 20 min to finish the Knoevenagel condensation. Subsequently, the autoclave was purged with H_2 for 4 times, and the H_2 pressure of the autoclave was set at 0.20 MPa for the subsequent hydrogenation process. The reaction solvent was magnetically stirred (245 rpm) at 50 ℃ for 3 h.

Catalytic of deacetalization-Knoevenagel cascade reaction. A mixture of benzaldehyde dimethylacetal (4 mmol), malononitrile (6 mmol), anhydrous toluene (8.0 mL), H_2O (0.2 mL) and the catalysts (0.2 g) was stirred at 80 ℃ for 3 h. The reaction conversion was calculated based on benzaldehyde dimethyl acetal since there was excess malononitrile. For the specified time, samples were taken periodically and analyzed by GC and GC-MS.

Results and Discussion

Study of the modified HPS structures. As shown in Fig. 1A and

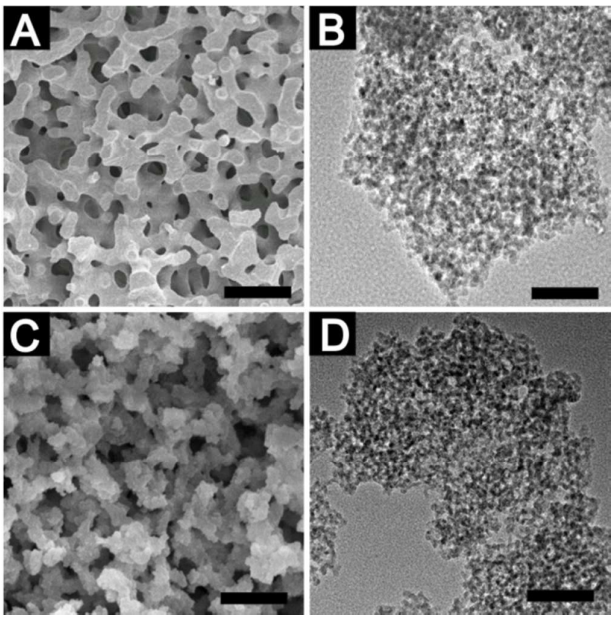

Fig. 1. SEM and TEM images of the HPS (A, B). SEM and TEM images of the HPS-PG (C, D). The scale bars in (A, C) represent 10 μm and the scale bars in (B, D) represent 100 nm.

View Article Online
DOI: 10.1039/C6RA12088A

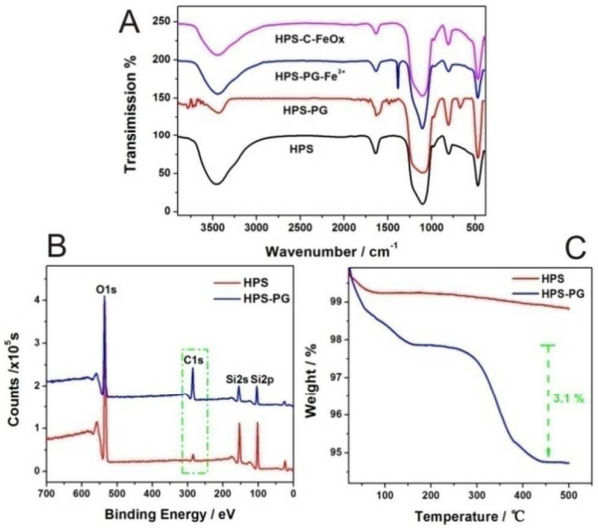

Fig. 2. (A) FT-IR spectra of HPS and modified process. (B) XPS spectrum of HPS before and after PG modification. (C) TGA plot of HPS before and after PG modification in flowing air from 25 to 500 ℃ to determine weight loss of 3.1 % (wt) upon oxidation of the PG layer.

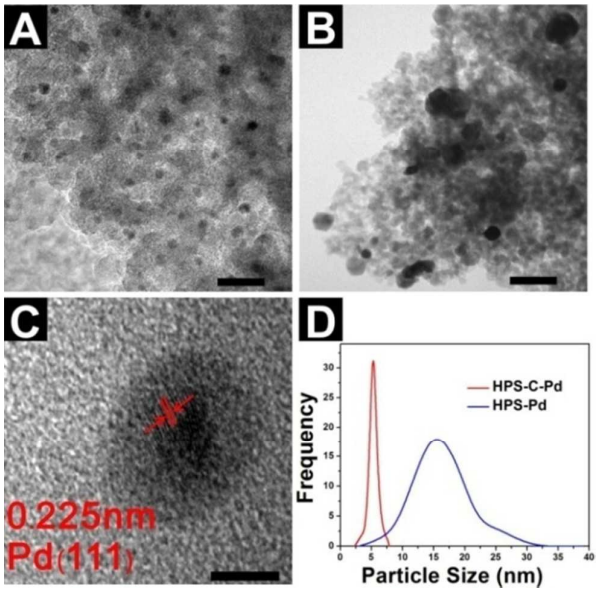

Fig. 3. TEM images of (A) HPS-C-Pd and (B) HPS-Pd and the scale bars represent 20 nm. HRTEM image of the (C) HPS-C-Pd nanocomposite and the scale bar represents 5 nm. (D) Pd particle size distributions were estimated by counting 55 particles in the the HPS-C-Pd TEM images and 48 particles in the HPS-Pd TEM images.

1B, the as-made HPS matrix exhibited an interconnected three-dimensional (3D) macroporous structure and abundant mesopores. The macropores and mesopores were about 2.3 μm and 14 nm in diameter, respectively. After modification with PG, the HPS-PG maintained its regular morphology without any blocking or cracking, and the texture of the silica skeleton turned slightly rougher, as shown in the SEM image (Fig. 1C). The mesopores were also well preserved according to the TEM image (Fig. 1D), indicating that the PG layer did not seriously affect the porous structure of the HPS.

The FT-IR, XPS and TGA results in Fig. 2 provide further evidence for the growth of PG on HPS. Fig. 2A shows that the bands around 1625-1400 cm^{-1} was assigned to the stretching vibrations of C=C in the benzene ring from the HPS-PG incomparison with the bare HPS, due to the formation of PG on the surface of the silica.[34] In the XPS curves (Fig. 2B), two high intensity peaks representing Si could be observed from the naked HPS at a binding energy of 150.5 eV (Si2s) and 100.2 eV (Si2p), respectively. Another two weak peaks at 532.7 eV and 284.8 eV were attributed to O1s and C1s, respectively.[35] After modification with PG, the Si2p peak from the silica substrate became weak. In contrast, the intensity of the C1s peaks was enhanced relative to Si2p. This indicated the formation of the PG coating on the HPS surface. The TGA plot of the HPS and HPS-PG (Fig. 2C) in flowing air from 25 to 500℃ and at around 100 ℃ were assigned to the absorbed water. The TGA curve of the HPS-PG was used to determine the weight loss upon oxidation of the PG, which was observed from 285 ℃ with a mass loss of about 3.1% (wt). This amount is close to that of a monolayer of PG molecules.

Inorganic compounds, including Pd, Al_2O_3, ZrO_2 and FeOx, were loaded onto the porous HPS and HPS-PG by impregnation and calcination, respectively. The TEM and SEM results show that the presence of PG obviously changed the dispersion state of the inorganics. Fig. 3A and 3B show the Pd loads of the HPS and HPS-PG, respectively. The PG layer allowed the Pd to form

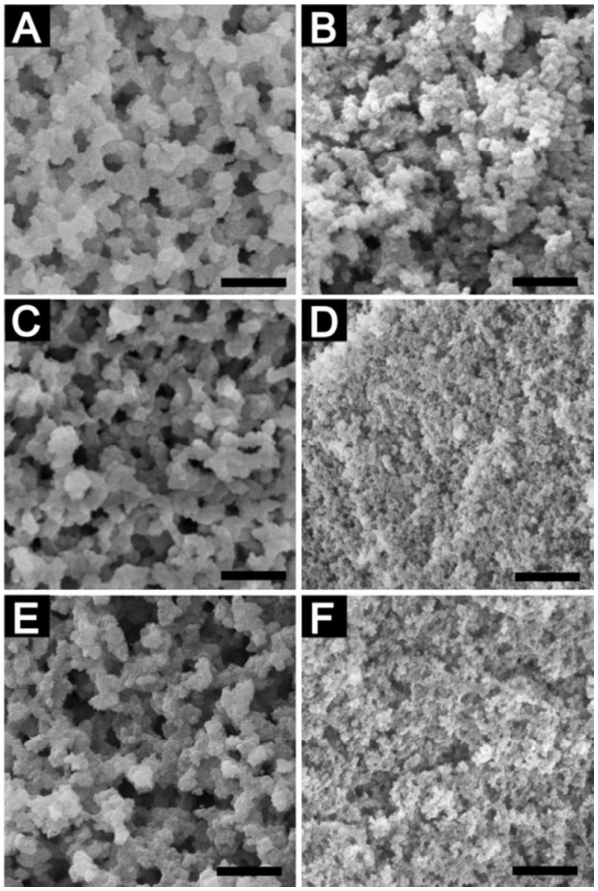

Fig. 4. SEM images of PG modified materials (A) HPS-C-FeOx (B) HPS-C-Al_2O_3 and (C) HPS-C-ZrO_2. The images in (B, D, E) are the corresponding uncoated silica HPS-FeOx, HPS-Al_2O_3 and HPS-ZrO_2, respectively. The scale bars in all of the images represent 10 μm.

View Article Online
DOI: 10.1039/C6RA12088A

small nanoparticles, which were highly dispersed in the porous silica. The high-resolution TEM image (Fig. 3C) shows small Pd particles with a well-defined crystalline structure with regular lattice spacing of d = 0.225 nm, consistent with the (111) lattice planes of the face centered cubic. As a comparison, Fig. 3B shows that quite large and non-uniform Pd particles formed on the bare HPS skeleton. The HPS-C-Pd (red line in Fig. 3D) had a narrower Pd particle size distribution with better dispersion and smaller Pd particles (5 ± 1.3 nm) with the help of the PG layer, whereas the HPS-Pd (blue line) had a broad Pd particle size distribution from 4 to 30 nm. These results were due to the reduction properties of the PG. Before calcination, the Pd^{2+} had already been partrly reduced to highly dispersed Pd nanoparticles on the surface of the porous material. In the conventional impregnation method, the nanoparticles formed during the calcination, making it difficult to control their size.

Further investigation of the specific effect of PG on metal oxides produced results similar to those for the above mentioned Pd particles. As shown in Fig. 4A, compared with the uncoated sample HPS-FeOx (Fig. 4B) , the skeleton of the HPS-C-FeOx become thick, but the material still had a better macroporous structure and less blocking, indicating that the PG played an important role in improving the dispersion of metal oxides after calcination. This result may be caused by the combination of the PG layer with the metal ions. It has been reported that polyphenol can coordinate with metal ions. To study the interactions between Fe^{3+} ions and PG polymer, FT-IR spectra analysis was conducted. As shown in Fig. 2A, after the HPS-PG adsorbed Fe^{3+} ions, a new sharp absorption band at 1384 cm^{-1} appeared, which was assigned to the stretching vibrations of C-O-Metal, confirming that the metal ions had coordinated with the hydroxyl groups.[36] The redundant ions caused by physical absorption were washed off and homodisperse metal oxides were obtained after calcination at 550 ℃. When Al_2O_3 and ZrO_2 were loaded onto the bare HPS and HPS-PG, the results were similar (Fig. 4C and 4D, and Fig. 4E and 4F, respectively), which were because of the PG helped highly dispersed metal oxides particles in the porous silica. After the modification of Al_2O_3 and ZrO_2, the blocking of pores in the bare HPS was so serious that virtually no macropores could be observed in the final products. This would be harmful for the transfer of reactants in the pores.

XPS was carried out to further analyze the surface composition of the synthesized component in the hierarchical porous silica (Fig. 5). A wide range XPS of the four examples (Fig. 5A, 5C, 5E and 5F) clearly shows four dominant peaks corresponding to C1s, O1s, Si2s and Si2p. These indicated the formation of the PG coating on the HPS surface. The XPS spectra for Pd 3d peak (Fig. 5B) can be de-convoluted into two pairs of doublets. A comparison of the relative areas of integrated intensity of Pd^0 and Pd^{2+} shows that the Pd mainly exists as Pd^0 in the HPS-PG-Pd (～68 %).[37, 38] This result confirms the generation of metallic Pd^0 particles and the reductive properties of PG. The high-resolution XPS spectra for Fe 2p is shown in Fig. 5D. Double peaks with binding energies of Fe $2p^{3/2}$ and Fe $2p^{1/2}$ at 711.1 and 724.9 eV are visible in the binding energy range of 705–735 eV. The satellite peak at

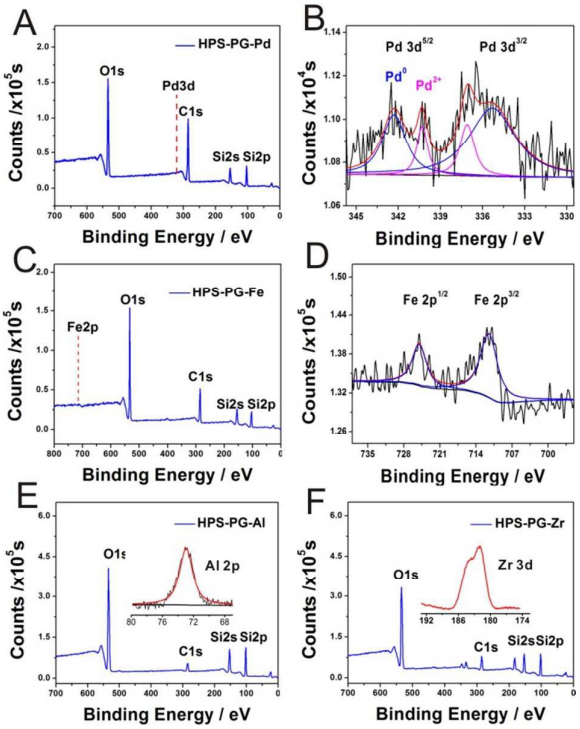

Fig. 5. XPS spectrum of HPS after surface modification. (A) typical XPS wide scan spectra of HPS-PG-Pd. (B) high-resolution XPS spectra of Pd 3d. (C) typical XPS wide scan spectra of HPS-PG-Fe. (D) high-resolution XPS spectra of Fe 2p and a shakeup satellite XPS peak observed between Fe $2p^{3/2}$ and Fe $2p^{1/2}$. (E) typical XPS wide scan spectra of HPS-PG-Al. Inset shows a spectra of Al 2p. (F) typical XPS wide scan spectra of HPS-PG-Zr. Inset shows a spectra of Zr 3d.

around 719 eV, which is typical of the maghemite phase, suggested the phase of the Fe_3O_4.[39, 40] In addition, XPS studies of HPS-PG-Al and HPS-PG-Zr confirmed the presence of aluminum and zirconia elements (inserts in Fig. 5E and 5F).[41, 42]

As Fig. 6 shows, the N_2 adsorption-desorption isotherms of the unmodified and modified HPS monoliths all belong to type-IV isotherm according to IUPAC classification.[43] It indicates that mesopores of HPS are maintained after modification. After loading the catalysts, the surface areas of all of the examples changed, as shown in Table 1. The HPS and HPS-PG had BET surface areas of 223.66 and 224.27 m^2 g^{-1} and pore volumes of

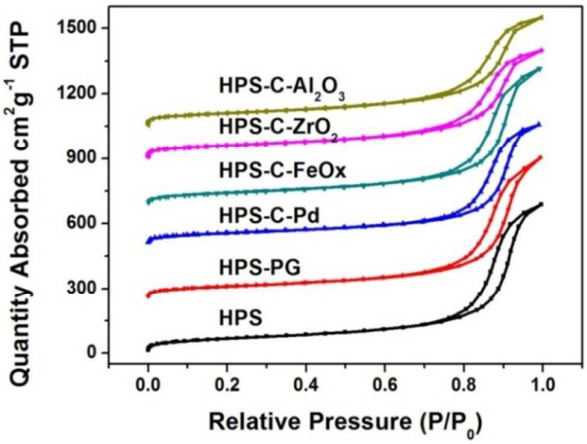

Fig. 6. N_2 adsorption-desorption isotherms of HPS, HPS-PG, and the subsequent modified materials.

View Article Online
DOI: 10.1039/C6RA12088A

Table 1. Structural properties of the HPS and modified HPS and the metal element content of various modified materials measured by ICP.

Sample	S_{BET} (m^2 g^{-1})	D_p (nm)	V_p (cm^3 g^{-1})	Metal element content (wt %)
HPS	223.66	14.16	1.069	--
HPS-PG	224.27	14.42	1.074	--
HPS-C-FeOx	204.51	13.87	0.919	5.74
HPS-C-Pd	213.6	13.67	0.942	0.129
HPS-C-Al_2O_3	223.26	13.92	1.052	0.142
HPS-C-ZrO_2	217.43	12.42	0.928	0.271

1.069 and 1.074 cm^3 g^{-1}, respectively, indicating that the thin PG layer did not block the pores in the HPS. The S_{BET} of different inorganics modified by HPS were about 204 to 220 m^2 g^{-1} and the pore size distribution before and after the modification of the HPS slight shrank from 14.16 to 11.07 nm and have uniform mesopores with narrow pore size distribution (as shown in Fig. S1), which were large enough for most organic molecules to diffuse through. The element content was measured using ICP-AES. The Fe content in the HPS-C-FeOx was 7.5 % (wt). The Pd, Al and Zr contents in the HPS-C-Pd, HPS-C-Al_2O_3 and HPS-C-ZrO_2 were 0.129% (wt), 0.142% (wt) and 0.271% (wt), respectively. The higher Fe content in the HPS-C-FeOx may have been induced by the reported stronger interaction between PG and Fe^{3+} ions.[44] These results indicate that the PG modified surface could effectively realize the immobilization of various kinds of inorganic catalysts with low loading amounts (less than 0.5% except for Fe).

Based on the outstanding performance of the PG layer for immobilizing inorganics, we attempted to integrate different components in a porous silica support by PG layer assisted LbL deposition. It is interesting that the LbL assembly was found to be beneficial for increasing the magnetics property of FeOx. The magnetic behavior of the samples was measured at 300 K in the applied magnetic field ranging from -20000 to 20000 Oe, as shown in Fig. 7. The asprepared HPS-Fe_2O_3 without the PG

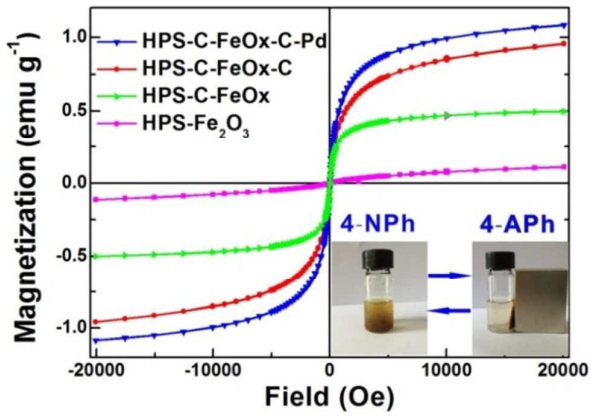

Fig. 7. Magnetization curves at 300 K in the applied magnetic field ranging from -20000 to 20000 Oe. The insert shows the magnetic separation-redispersion process of the HPS-C-FeOx-C-Pd catalyzed 4-nitrophenol (4-NPh) to 4-aminophenol (4-APh).

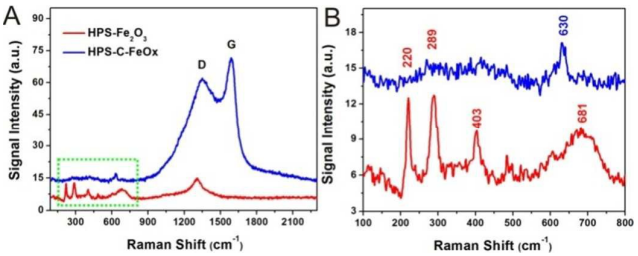

Fig. 8. (A) Raman spectra of the HPS-Fe_2O_3 (red) and HPS-C-FeOx (blue) nanocomposites. (B) magnification image of the green rectangular area in (A). The red line is hematite based on the characteristic peaks at 220, 289, 403, 681 and 1316 cm^{-1}; the blue line is magnetite, as revealed by the peaks at 630 cm^{-1}. Raman spectra were collected at room temperature.

layer behaved as a weak paramagnet displaying no saturation or coercivity (Fig. S2). In the presence of the PG layer, the saturation magnetization value of HPS-C-FeOx was 0.46 emu g^{-1}. After immobilization and calcination of the PG twice, the magnetization of the samples increased from 0.46 to 0.95 emu g^{-1}.

Raman spectroscopy was used to confirm the type of magnetic FeOx in the porous silica. Fig. 8 presents the in situ Raman spectra of HPS-Fe_2O_3 and HPS-C-FeOx. HPS-Fe_2O_3 exhibits five bands, 220, 289, 403, 681 and 1316 cm^{-1}, which are typical γ -Fe_2O_3 features.[45] The additional typical peak at 630 cm^{-1}, for HPS-C-FeOx, probably because of the surface Fe^{3+} was partially reduced to Fe^{2+} due to the reducing property of PG to form Fe_3O_4. This suggests that the systematic increase in the saturated magnetization was due to the increased Fe_3O_4 content in the samples.[46] The immobilized Pd greatly enhanced the magnetization to a higher degree, reaching 1.01 emu g^{-1}. This result is in agreement with earlier reports that the noble metal induced the reduction of the non-noble metal

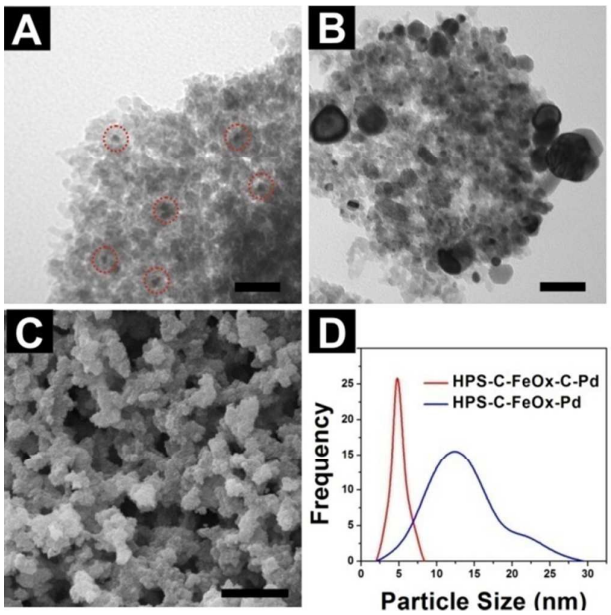

Fig. 9. TEM images of (A) the HPS-C-FeOx-C-Pd and (B) the HPS-C-FeOx-Pd and the scale bars represent 20 nm. (C) SEM image of the HPS-C-FeOx-C-Pd nanocomposite and the scale bar represents 10 μm. (D) Pd particle size distributions were estimated by counting 45 particles in the the HPS-C-FeOx-C-Pd TEM images and 36 particles in the HPS-C-FeOx-Pd TEM images.

View Article Online
DOI: 10.1039/C6RA12088A

ions by reducing agent.[47, 48] Herein, the noble metal was Pd^{2+}, the non-noble metal ion was Fe^{3+} and the reductant should have been PG. As shown in the inset of Fig. 7, the HPS-C-FeOx-C-Pd aggregated within a few seconds after an external magnetic field was applied, redispersed quickly again via shaking when the magnetic field was removed, demonstrating the magnetic separation property of the material, which is particularly desirable for its practical applications in catalysis. The Raman spectrum of the HPS-C-FeOx (Fig. 8A) is used to further investigat the transformation of the PG layer to carbon on the silica support. The broad Raman bands (Fig. 8A) appearing at 1340 cm^{-1} (denoted as D-band) generally refer to the sp^2 planar and conjugated structures.[49] The narrow G-band appearing at 1585 cm^{-1} indicates a disordered graphitic structure. The D/G ratio (~0.84) is slightly smaller than the reported values of TiO_2@Carbon prepared by the in situ polymer encapsulation–graphitization method, which is indicative of the transformation of the PG layer to carbon.[50]

The effect of FeOx on the loading of other components was examined. Fig. 9A and 9B show the corresponding TEM images of the HPS-C-FeOx-C-Pd and HPS-C-FeOx-Pd and the results are the same as in Fig. 3A and 3B. The HPS-C-FeOx-C-Pd, which was produced by the PG assisted LbL deposition, showed high Pd dispersion compared with the non-PG-coated HPS-C-FeOx. Other bi- and multi-functional catalysts based on the magnetic carrier were prepared by the LbL coating. The N_2 sorption isotherms of the catalysts are shown in Fig. S3. The pore diameter and pore volume showed few changes, and the values were similar to the bare HPS (Table S1). The LbL coating bi- and multi-functional materials still had better macroporous structures and less blocking (as shown in Fig. S4), which may have been caused by the low loading amounts of the elements. Therefore, the LbL coating process does not induce the pore blocking of the support materials, and can ensure the transfer of substances during the catalytic reaction.

Study of catalytic performance of modified HPS. The catalytic activity of the obtained catalysts was explored through rapid Suzuki Miyaura coupling reaction, Knoevenagel condensation, Friedel–Crafts alkylation, nitrophenol reduction reaction and cascade reactions. The catalytic activity of the Pd loaded catalyst was examined in one of the representative Pd catalyzed Suzuki Miyaura coupling reactions and the results are summarized in Table 2. The different catalyst design strategies show different catalytic activity. The TOF for the HPS-C-Pd and HPS-C-FeOx-C-Pd (Entry 1, 3) is higher, representing a 2-4 times improvement over the other catalysts (Entry 2, 4). The PG coating thus represents a novel approach to achieving the high dispersion of Pd nanoparticles. Given a similar Pd content, the smaller particle size leads to a larger exposed surface area and high reactivity.

The multicomponent catalysts, which contained Al_2O_3 or ZrO_2, exhibited similar results to those of the above mentioned Pd catalyst. In the Al_2O_3-catalyzed Knoevenagel condensation method (Table 3), the deposited PG layer played an important role in improving the dispersion of catalysts, therefore, led to a higher TOF value representing a 2-4 times improvement over

Table 2. Catalytic activity test of various Pd catalysts in the Suzuki-Miyaura coupling reaction of iodobenzene and phenylboronic acid.

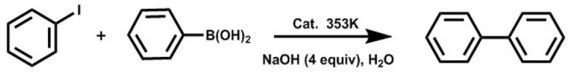

Entry	Cat.	Pd counts (wt %)	Time (h)	Conv. (%)	TOF (h^{-1})
1	HPS-C-Pd	0.1288	3	99	272.7
2	HPS-Pd	0.1162	4	33	75.5
3	HPS-C-FeOx-C-Pd	0.1377	2.5	99	306.1
4	HPS-C-FeOx-Pd	0.1305	4	68	138.6

Reaction condition: iodobenzene (2 mmol), phenylboronic acid (2.4 mmol), NaOH (8 mmol) and Cat. (0.2 g). TOF was calculated by moles of product per molar Pd per hour. Conversion was determined by GC and the product were determined by the GC-MS and the ^{1}H NMR spectrum (400 MHz, CD_3CN) which are included in Fig. S5, Fig. S6 and Fig. S7 in the Supporting Information.

Table 3. Catalytic activity test of various Al_2O_3 catalysts in the Knoevenagel condensations of benzaldehyde and ethyl cyanoacetate or malonitrile.

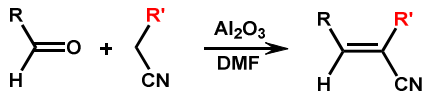

Entry	Cat.	Al Counts (wt %)	[a]R′ Conv. (%)	[a]R′ TOF (h^{-1})	[b]R′ Conv. (%)	[b]R′ TOF (h^{-1})
1	HPS-C-Al_2O_3	0.1417	99	419.2	100	9432.0
2	HPS-Al_2O_3	0.2901	46	95.2	52	2396.5
3	HPS-C-FeOx-C-Al_2O_3	0.1735	99	342.4	99	7626.2
4	HPS-C-FeOx-Al_2O_3	0.1928	57	177.4	58	4020.6

[a]**Reaction condition:** benzaldehyde (0.1 mol), ethyl cyanoacetate (0.11 mol), DMF (15 mL) and Cat. (0.5 g) at 80 ℃ for 9 h. [b]Reaction condition: benzaldehyde (0.1 mol), malonitrile (0.11 mol), DMF (15 mL) and Cat. (0.25 g) at 25 ℃ for 1 h. Conversion was determined by GC and the product were determined by the GC-MS and the ^{1}H NMR spectrum (400 MHz, CD_3CN) which are included in Fig. S8 - Fig. S13 in the Supporting Information.

Table 4. Friedel–Crafts alkylation of indoles with chalcones catalyzed by various ZrO_2 catalysts.

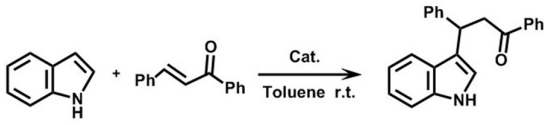

Entry	Cat.	Zr Counts (wt %)	Conv. (%)	TOF (h^{-1})
1	HPS-C-ZrO_2	2.272	99	13.2
2	HPS-ZrO_2	2.315	32	6.9
3	HPS-C-FeOx-C-ZrO_2	1.908	~100	15.7
4	HPS-C-FeOx-ZrO_2	2.012	56	8.4

Reaction condition: indoles (2 mmol), chalcones (3 mmol), methylbenzene (20mL) and Cat. (0.1 g) at 110 ℃. Values at t = 6 h. Conversion was determined by GC and the product were determined by the GC-MS and the ^{1}H NMR spectrum (400 MHz, CD_3CN) which are included in Fig. S14 - Fig. S16 in the Supporting Information.

View Article Online
DOI: 10.1039/C6RA12088A

Table 5. One-Pot Knoevenagel condensation–hydrogenation multistep cascade reaction (a) and tandem Deacetalization Knoevenagel condensation (b) catalyzed by various multi-functional catalysts.

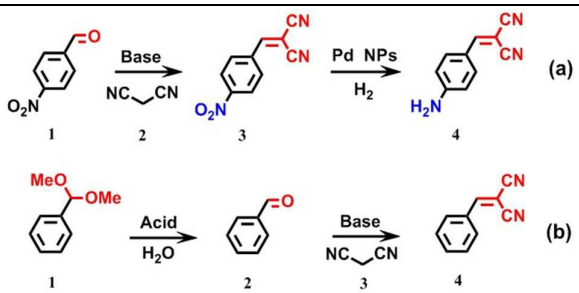

Entry	Cat.	(a)			(b)		
		Conv. of 1 (%)	Yield of 3 (%)	Yield of 4 (%)	Conv. of 1 (%)	Yield of 2 (%)	Yield of 4 (%)
1	HPS	17	17	Trace	~3	Trace	Trace
2	HPS-C-Al_2O_3	~99	99	Trace	22	1	21
3	HPS-C-Pd	22	1	21	---	---	---
4	HPS-C-Al_2O_3-C-Pd	~100	1	99	---	---	---
5	HPS-C-FeOx-C-Al_2O_3-C-Pd	~100	Trace	~100	---	---	---
6	HPS-C-ZrO_2	---	---	---	99	86	13
7	HPS-C-Al_2O_3-C-ZrO_2	---	---	---	99	2	97
8	HPS-C-FeOx-C-Al_2O_3-C-ZrO_2	---	---	---	~100	Trace	~100

[a]**Reaction condition:** 4-nitrobenzaldehyde (0.2 mmol) , malononitrile (0.21 mmol), DMF (15 mL) and Cat. (0.2 g) with H_2 pressure 0.2 MPa, stirred (245 rmp) at 80 ℃ for 3 h. [b]Reaction condition: benzaldehyde dimethylacetal (4 mmol) malononitrile (6 mmol), H_2O (0.2 mL) and toluene (5 mL) at 80 ℃ for 3 h. Conversion was determined by GC and the product were determined by the GC-MS and the ^{1}H NMR spectrum (400 MHz, CD_3CN) which are included in Fig. S17 - Fig. S22 in the Supporting Information.

the traditional impregnation method catalyst. The HPS-C-FeOx-C-ZrO_2 was evaluated by catalyzing the Friedel–Crafts alkylation (Table 4), which retained higher activity and a TOF value 2 times that of the HPS-C-FeOx-ZrO_2. The ICP results showed that the content of the catalytic compounds did not vary too much in the different catalysts. The Al and Zr elements were even smaller in the LbL-prepared catalysts. All of these results indicate that the PG-coated materials led to higher efficiency due to the high dispersion and stability of the active metal oxides. In addition, no catalysts were observed in the filtrate at the detectable limits of ICP. These results show that there was little leaching, which contributed to the stability and recyclability of the catalyst.

To further improve the multi-functional features of the catalyst, we successfully combined two types of catalytic active sites with magnetic response properties on a single platform with the help of PG layers using the LbL coating method. These novel magnetically recyclable heterogeneous catalysts exhibited superior catalytic performance for one-pot cascade reactions, such as the Knoevenagel condensation-hydrogenation cascade reaction and deacetalization-Knoevenagel cascade reaction. The results showed that 99% yield of the final product with 100% selectivity was achieved after 3 h, indicating that the tandem reaction (Knoevenagel condensation-hydrogenation hybrid catalysts) was successful. Similar yields (acid-base hybrid catalysts) of the final product were observed for the other one-pot reaction (Table 5) with the same reaction time. A blank experiment without the heterogeneous catalyst was also performed (entry 1), and the results showed that the cascade reaction yield was only a trace in the absence of the hybrid catalyst.

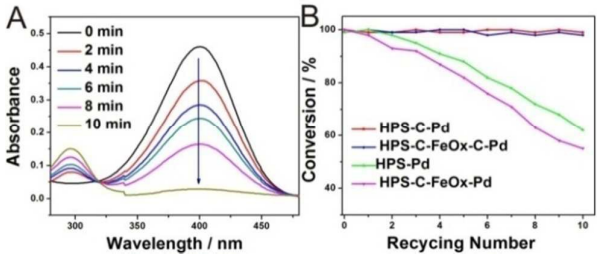

Fig. 10. (A) Time-dependent evolution of UV–vis absorption spectra showing 4-NPh to 4-APh catalyzed by HPS-C-FeOx-C-Pd at room temperature. (B) Recycling performance of the four catalysts.

The catalysts have the important characteristics of easy recycling and reusability. As Fig. 10A shows, the modified samples revealed a complete conversion of 4-NPh to 4-APh within 10 min. To determine the durability of the catalyst, it was recovered by simple magnetic separation and subsequently reused after regeneration. After 10 cycles, the conversion rate was still higher than 99% (Fig. 10B). The samples without the help of PG were reused, but showed an obvious loss of catalytic activity, with the conversion rate reduced to about 60% after 10 cycles. This indicates that the PG layer helps to stabilize the catalysts even though the layer changes to carbon with the following calcination. The carbon coating catalysts retained higher activity and demonstrated

View Article Online
DOI: 10.1039/C6RA12088A

improved stability compared with the uncoated catalysts. It may also be possible to functionalize the carbon to provide additional improvements in catalytic performance.

Conclusions

In summary, we present a general chemical approach for improving the traditional method of preparing catalysts loaded on porous silica, using PG, a polyphenol from plants. The PG layer, when adhered to the surface of silica, remarkably reduces the particle size of the catalysts and increases their dispersion, which helps to avoid the blocking of the pores in the silica support. Furthermore, the reducibility and adhesiveness of the PG layer allows various magnetic and catalytic inorganics to be successfully immobilized on the surface of the support by the biomineralization. The PG acts as both an adsorbing agent and a reducing agent, resulting in a multifunctional catalyst containing highly dispersed catalytic active sites and magnetic response properties. It shows excellent catalytic activity in the Suzuki Miyaura coupling reaction, nitrophenol reduction reaction, Knoevenagel condensation reaction and Friedel-Crafts alkylation. The TOF values are several times higher than those achieved by the normal impregnation method. More importantly, this catalyst can be easily recycled and reused, thus showing good potential for practical applications. The strategy presented here, which uses a PG layer to achieve the LbL coating, can be used to adjust the surface environment of the conventional support material and help to overcome some of the agglomeration of particles. Furthermore, these magnetically recoverable catalysts provide a solid and stable platform for heterogeneous catalysis and green chemistry in the near future.

Acknowledgements

This work was supported by National Natural Science Foundation of China (21473019, 51273030) and the Fundamental Research Funds for the Central Universities (DUT14ZD217).

Notes and references

1 X. F. Yang, A. Q. Wang, B. T. Qiao, J. Li, J. Y. Liu and T. Zhang, *Accounts Chem. Res.*, 2013, **46**, 1740-1748.
2 S. Wang, Q. F. Zhao, H. M. Wei, J. Q. Wang, M. Y. Cho, H. S. Cho, O. Terasaki and Y. Wan, *J. Am. Chem. Soc.*, 2013, **135**, 11849-11860.
3 J. Liu, S. Z. Qiao, S. B. Hartono and G. Q. Lu, *Angew. Chem. Int. Edit.*, 2010, **49**, 4981-4985.
4 H. Duan, M. H. Li, G. H. Zhang, J. R. Gallagher, Z. L. Huang, Y. Sun, Z. Luo, H. Z. Chen, J. T. Miller, R. Q. Zou, A. W. Lei and Y. L. Zhao, *ACS Catal.*, 2015, **5**, 3752-3759.
5 H. S. Wei, X. Y. Liu, A. Q. Wang, L. L. Zhang, B. T. Qiao, X. F. Yang, Y. Q. Huang, S. Miao, J. Y. Liu and T. Zhang, *Nat. Commun.*, 2014, **5**, 8.
6 Y. Ma, L. Xu, W. Chen, C. Zou, Y. Yang, L. Zhang and S. Huang, *RSC Adv.*, 2015, **5**, 103797-103802.
7 N. Fan, Y. Yang, W. Wang, L. Zhang, W. Chen, C. Zou and S. Huang, *ACS Nano*, 2012, **6**, 4072-4082.
8 Y. Yang, W. Wang, X. Li, W. Chen, N. Fan, C. Zou, X. Chen, X. Xu, L. Zhang and S. Huang, *Chem. Mat.*, 2013, **25**, 34-41.
9 L. Srisombat, A. C. Jamison and T. R. Lee, *Colloid Surf. A-Physicochem. Eng. Asp.*, 2011, **390**, 1-19.
10 H. N. Pham, A. E. Anderson, R. L. Johnson, T. J. Schwartz, B. J. O'Neill, P. Duan, K. Schmidt-Rohr, J. A. Dumesic and A. K. Datye, *ACS Catal.*, 2015, **5**, 4546-4555.
11 H. Y. Liu, L. Y. Zhang, N. Wang and D. S. Su, *Angew. Chem. Int. Edit.*, 2014, **53**, 12634-12638.
12 W. Jing, L. Yuyun, C. Jia, L. Yuhui, Y. Qin, P. Gaoxiang, Y. Yanlei, D. Yonghui and Z. Dongyuan, *Adv. Mater.*, 2014, **26**, 1782-1787.
13 Y. Wang, R. Q. Huang, G. H. Liang, Z. Y. Zhang, P. Zhang, S. N. Yu and J. L. Kong, *Small*, 2014, **10**, 109-116.
14 Y. Lee and T. G. Park, *Langmuir*, 2011, **27**, 2965-2971.
15 F. Zhang, H. Y. Jiang, X. Y. Li, X. T. Wu and H. X. Li, *ACS Catal.*, 2014, **4**, 394-401.
16 M. T. Zhao, K. Deng, L. C. He, Y. Liu, G. D. Li, H. J. Zhao and Z. Y. Tang, *J. Am. Chem. Soc.*, 2014, **136**, 1738-1741.
17 H. Wang, J. J. Wu, C. Cai, J. Guo, H. S. Fan, C. Z. Zhu, H. X. Dong, N. Zhao and J. Xu, *ACS Appl. Mater. Interfaces*, 2014, **6**, 5602-5608.
18 H. Lee, S. M. Dellatore, W. M. Miller and P. B. Messersmith, *Science*, 2007, **318**, 426-430.
19 H. Y. Liu and N. F. Hu, *J. Phys. Chem. B*, 2005, **109**, 10464-10473.
20 R. R. Xing, T. F. Jiao, L. Y. Yan, G. H. Ma, L. Liu, L. R. Dai, J. B. Li, H. Mohwald and X. H. Yan, *ACS Appl. Mater. Interfaces*, 2015, **7**, 24733-24740.
21 S. H. Lee, A. C. Jamison, D. M. Hoffman, A. J. Jacobson and T. R. Lee, *Thin Solid Films*, 2014, **558**, 200-207.
22 S. S. Shankar, A. Rai, B. Ankamwar, A. Singh, A. Ahmad and M. Sastry, *Nat. Mater.*, 2004, **3**, 482-488.
23 Y. Ji, L. Huang, J. Hu, C. Streb and Y.-F. Song, *Energy Environ. Sci.*, 2015, **8**, 776-789.
24 E. K. Jeon, E. Seo, E. Lee, W. Lee, M.-K. Um and B.-S. Kim, *Chemical communications*, 2013, **49**, 3392-3394.
25 Y. Long, K. Liang, J. Niu, X. Tong, B. Yuan and J. Ma, *New J. Chem.*, 2015, **39**, 2988-2996.
26 J. Luo, N. Zhang, R. Liu and X. Liu, *RSC Adv.*, 2014, **4**, 64816-64824.
27 G. Liu, D. Wang, F. Zhou and W. Liu, *Small*, 2015, **11**, 2807-2816.
28 C. Wang, J. Chen, X. Zhou, W. Li, Y. Liu, Q. Yue, Z. Xue, Y. Li, A. A. Elzatahry, Y. Deng and D. Zhao, *Nano Research*, 2014, **8**, 238-245.
29 A. Meffre, B. Mehdaoui, V. Connord, J. Carrey, P. F. Fazzini, S. Lachaize, M. Respaud and B. Chaudret, *Nano letters*, 2015, **15**, 3241-3248.
30 Z. Sun, Q. Yue, Y. Liu, J. Wei, B. Li, S. Kaliaguine, Y. Deng, Z. Wu and D. Zhao, *J. Mater. Chem. A*, 2014, **2**, 18322-18328.
31 G. Cui, Z. Sun, H. Li, X. Liu, Y. Liu, Y. Tian and S. Yan, *J. Mater. Chem. A*, 2016, **4**, 1771-1783.
32 T. S. Sileika, D. G. Barrett, R. Zhang, K. H. A. Lau and P. B. Messersmith, *Angewandte Chemie International Edition*, 2013, **52**, 10766-10770.
33 S. Y. Tao, Y. C. Wang, D. Shi, Y. L. An, J. S. Qiu, Y. S. Zhao, Y. Cao and X. F. Zhang, *J. Mater. Chem. A*, 2014, **2**, 12785-12791.
34 H. Kawakita, S. Nakano, K. Hamamoto, Y. Matsunaga, Y. Yoshimura, K. Ohto and K. Inoue, *J. Appl. Polym. Sci.*, 2010, **118**, 247-252.
35 Q. Liu, N. Y. Wang, J. Caro and A. S. Huang, *J. Am. Chem. Soc.*, 2013, **135**, 17679-17682.
36 S. Y. Tao, P. Fan, Y. C. Wang, C. Wang, T. Hu and C. G. Meng, *J. Mater. Chem. C*, 2014, **2**, 1962-1965.

View Article Online
DOI: 10.1039/C6RA12088A

37 M. H. Tang, S. J. Mao, M. M. Li, Z. Z. Wei, F. Xu, H. R. Li and Y. Wang, *ACS Catal.*, 2015, **5**, 3100-3107.
38 E. Karakhanov, A. Maximov, Y. Kardasheva, V. Semernina, A. Zolotukhina, A. Ivanov, G. Abbott, E. Rosenberg and V. Vinokurov, *ACS Appl. Mater. Interfaces*, 2014, **6**, 8807-8816.
39 S. Venkateswarlu and M. Yoon, *ACS Appl. Mater. Interfaces*, 2015, **7**, 25362-25372.
40 R. Z. Li, Y. M. Wang, C. Zhou, C. Wang, X. Ba, Y. Y. Li, X. T. Huang and J. P. Liu, *Adv. Funct. Mater.*, 2015, **25**, 5384-5394.
41 L. H. Kim, K. Kim, S. Park, Y. J. Jeong, H. Kim, D. S. Chung, S. H. Kim and C. E. Park, *ACS Appl. Mater. Interfaces*, 2014, **6**, 6731-6738.
42 Y. H. Pan, Y. Gao, D. D. Kong, G. D. Wang, J. B. Hou, S. W. Hu, H. B. Pan and J. F. Zhu, *Langmuir*, 2012, **28**, 6045-6051.
43 M. Vila, J. L. Hueso, M. Manzano, I. Izquierdo-Barba, A. de Andres, J. Sanchez-Marcos, C. Prieto and M. Vallet-Regi, *Journal of Materials Chemistry*, 2009, **19**, 7745-7752.
44 W. E. L. Santana, C. V. Nunez and H. D. Moya, *Nat. Prod. Commun.*, 2015, **10**, 1821-1824.
45 C. Pascal, J. L. Pascal, F. Favier, M. L. E. Moubtassim and C. Payen, *Chem. Mat.*, 1999, **11**, 141-147.
46 P. Li, Y. Yu, H. Liu, C. Y. Cao and W. G. Song, *Nanoscale*, 2014, **6**, 442-448.
47 D. Wang and Y. Li, *Adv Mater*, 2011, **23**, 1044-1060.
48 S. F. Cai, H. H. Duan, H. P. Rong, D. S. Wang, L. S. Li, W. He and Y. D. Li, *ACS Catal.*, 2013, **3**, 608-612.
49 Q. T. Qu, J. M. Chen, X. X. Li, T. Gao, J. Shao and H. H. Zheng, *J. Mater. Chem. A*, 2015, **3**, 18289-18295.
50 Z. Li-Wu, F. Hong-Bo and Z. Yong-Fa, *Adv. Funct. Mater.*, 2008, **18**, 2180-2189.

View Article Online
DOI: 10.1039/C6RA12088A

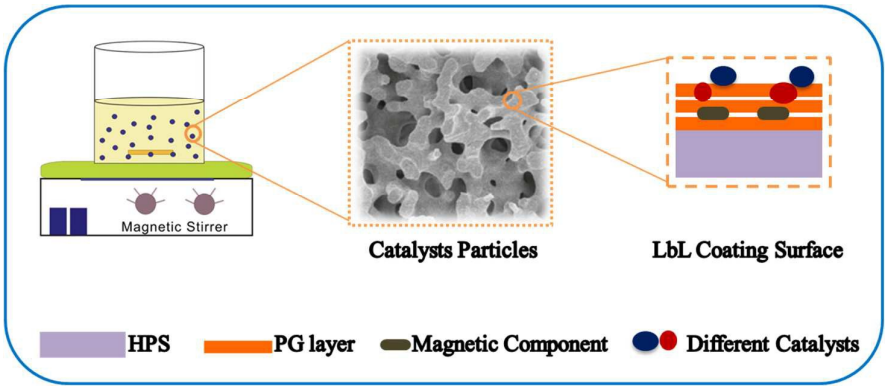

A facile synthetic approach for preparing magnetic porous catalysts, on which various inorganic compounds loaded by pyrogallic acid (PG) assisted layer-by-layer (LbL) coating.